Journal of Organometallic Chemistry 695 (2010) 580–587

Contents lists available at ScienceDirect

Journal of Organometallic Chemistry

journal homepage: www.elsevier.com/locate/jorganchem

Rare-earth (Eu^{3+}, Tb^{3+}) hybrids through amide bridge: Chemically bonded self-assembly and photophysical properties

Jinliang Liu, Bing Yan *

Department of Chemistry, Tongji University, Siping Road 1239, Shanghai 200092, PR China

ARTICLE INFO

Article history:
Received 1 September 2009
Received in revised form 30 October 2009
Accepted 6 November 2009
Available online 12 November 2009

Keywords:
Rare-earth hybrid material
Chemically bonded self-assembly
Photophysical property

ABSTRACT

This work focuses on the construction of a series of chemically bonded rare-earth/inorganic/organic hybrid materials (TCH–Si–Ln, TCH–Si–Ln–Phen and TCH–Si–Ln–Bipy: Phen = 1,10-phenanthroline, Bipy = 2,2′-bipyridyl) using TCH–Si as an organic bridge molecule that can both coordinate to rare-earth ions (Eu^{3+} and Tb^{3+}) and form an inorganic Si–O–Si network with tetraethoxysilane (TEOS) after cohydrolysis and copolycondensation through a sol–gel process. All of these hybrid materials exhibit homogeneous microstructures and morphologies, suggesting the occurrence of self-assembly of the inorganic network and organic chain. Measurements of the photoluminescent properties of these materials show that the ternary europium systems present stronger luminescent intensities than the binary hybrids, indicating that the introduction of the second ligands can sensitize the luminescence emission of the europium hybrid systems. However, in the terbium systems, this phenomenon was not observed.

1. Introduction

Luminescent lanthanide complexes have attracted special attention in recent years due to their academic interests and potential applications in a wide variety of photonic utilities [1–3]. Among the Ln^{3+} compounds, Eu^{3+} and Tb^{3+} ions are the most two popular Ln^{3+} ions because of their sharp characteristic emissions in red and green region, which can be used as emitters of electroluminescent devices and photoluminescent markers, labels of fluoroimmunoassay and so on [4,5]. In those compounds, the emission of Eu^{3+} or Tb^{3+} complexes usually results from the so-called "antenna effect", which is defined as a light conversion process via an energy absorption, energy-transfer and emission sequence. In such a process, the organic ligands act as photosensitizers or antenna chromophores to absorb and transfer the energy of light to excite the lanthanide ions via an energy-transfer process [6,7]. Due to the versatility in organic synthesis, the luminescent properties of lanthanide complexes can be custom-tailored depending on the desired application. The research in chromophores' design seems to be shifting to the optimization of a variety of other parameters, i.e. thermal stability, chemical resistance and optical transparence [8–10]. As a consequence, it comes up the possibility to generate new materials which are known as organic–inorganic hybrid materials [11,12]. Organic–inorganic hybrid materials have attracted special attention in recent years due to their interesting properties because they combine the two or more integrating components at the molecular or nanometer level and thus they can be specially tailored to give desirable properties or to suppress undesirable ones for wide-ranging applications [13,14]. The silica network can provide good mechanical resistance, extraordinary thermal stability and entirely amorphous systems, so the incorporation of organic compounds into silica gels and glasses is of the utmost interest for a variety of organic–inorganic hybrid materials, including optical devices [15–17]. According to the types of chemical interactions between the organic and the inorganic components, the hybrids can be categorized into two main classes [18]: Class I materials concerns the conventional doping systems in which only weak interactions (such as hydrogen bonding, van der Waals forces, or electrostatic forces) exist between organic and inorganic moieties. Class II materials belong to the molecule-based composite materials in which the organic and inorganic phases are linked together through strong chemical interactions (covalent, ion or coordination bonds). In these materials, the organic group is covalently bonded to the trifunctional silicon groups through Si–C bonds and then embedded into the Si–O–Si matrixes after hydrolysis and polycondensation processes, thus makes the organic group an integral part of the materials. So, the design of a functional bridge molecule (precursor), which can behave double functions of coordinating to rare-earth ions and allowing sol–gel process to constitute covalent Si–O networks, by the grafting reaction, has become the key procedure to construct such molecule-based materials [19–23]. Our research group recently put more emphasis on the preparation of functional systems covalently connecting both the siliceous backbone and photoactive units. We have successfully realized six paths to construct the functional

* Corresponding author. Tel.: +86 21 65984663; fax: +86 21 65982287.
E-mail address: byan@tongji.edu.cn (B. Yan).

0022-328X/$ - see front matter © 2009 Elsevier B.V. All rights reserved.
doi:10.1016/j.jorganchem.2009.11.005

silylated precursors, which are the modifications of amine groups [24], carboxyl groups [25], hydroxyl groups [26–28], sulfonic groups [29], mercapto groups [30,31] and methylene groups [32]. After the modification, we assembled the above modified bridge ligands with lanthanide ions and tetraethoxysilane (TEOS) to compose hybrid systems with covalent-bonds and obtained a series of stable and efficient molecular hybrid materials in optical areas.

Based on the former work, in this paper, we first synthesized the organic compound thiocarbohydrazide (denoted as TCH) containing two amine groups. And then we grafted the compound TCH to 3-(triethoxysilyl)propyl isocyanate (denoted as TESPIC) by amine group modification to achieve a molecular precursor (denoted as TCH–Si) through the hydrogen-transfer nucleophilic addition reaction between the amine group of TCH and the isocyanate group of TESPIC. Then, we prepared a series of chemically bonded rare-earth/inorganic/organic hybrid materials (denoted as TCH–Si–Ln) using TCH–Si as the bridge molecule that can both coordinate to rare-earth ions (Eu^{3+} and Tb^{3+}) and form inorganic Si–O–Si networks with tetraethoxysilane (TEOS) after cohydrolysis and copolycondensation processes. Further, in order to study the influence of the addition of the second ligands (1,10-phenanthroline, denoted as Phen, and 2,2′-bipyridyl, denoted as Bipy) to the luminescent intensities of the above binary hybrids, we also prepared two types of ternary rare-earth/inorganic/organic hybrids (denoted as TCH–Si–Ln–Phen and TCH–Si–Ln–Bipy) by the introduction of the second ligands (Phen and Bipy) into the above system. Comparison of performances of TCH–Si–Lanthanide systems with those of our previous materials [24–32], these TCH–Si–Ln hybrids can exhibit a high thermal stability, strong fluorescent intensities and high quantum efficiencies especially after the addition of Phen. Besides, the hybrid materials demonstrate that a homogeneously and uniformly system was obtained and no phase separation could be observed.

2. Experimental

2.1. Materials

Starting materials were purchased from Sinopharm Chemical Reagent Co., Ltd. (SCRC). All the reagents are analytically pure. These solvents were purified according to the literature procedures [33]. Other starting reagents were used as received. Europium and terbium nitrates were obtained by dissolving Eu_2O_3 and Tb_4O_7 in concentrated nitric acid, respectively. Tetraethoxysilane (TEOS) was distilled and stored under a N_2 atmosphere.

2.2. Synthesis

The synthesis procedure of the organic compound thiocarbohydrazide (TCH) and the silylated precursor (TCH–Si) were shown in Fig. 1A.

2.2.1. Synthesis of thiocarbohydrazide (TCH)

About 40 mL of 85% hydrazine hydrate was dissolved in 120 mL of water, and then 12 mL of CS_2 was added dropwise, the reaction mixture was kept under room temperature for 1 h and then heated to 363 K for additional 10 h. After cooling, the precipitate was filtered off, washed with water and dried under room temperature. The crude product was purified by recrystallization form water and finally obtained as white needles, yield 12.04 g (72%). m.p. 172–173 °C. ^{1}H NMR (DMSO, 500 MHz): δ 4.48 (d, 4H, NH_2); 8.69 ppm (t, 2H, NH). Elemental Anal. Calc. for CH_6N_4S: C, 11.31; H, 5.70; N, 52.78. Found: C, 11.23; H, 5.82; N, 52.70%.

2.2.2. Synthesis of the precursor TCH–Si

About 2 mmol of TCH was dissolved in 10 mL of tetrahydrofuran (THF), the resulting mixture was heated under reflux, and then 3-(triethoxysilyl)-propyl isocyanate (2 mmol) dissolved in 10 mL of THF was added dropwise. The mixture was warmed at 343 K for approximately 12 h under argon in a covered flask. After cooling, the solvent was removed in vacuo, and the residue was washed with 10 mL of hexane three times then clear oil was obtained in a 94.6% yield. ^{1}H NMR ($CDC1_3$, 500 MHz): 0.63 (t, 4H, CH_2Si); 1.22 (t, 18H, CH_3CH_2); 1.65 (m, 4H, $CH_2CH_2CH_2$); 2.12 (s, 2H, CSNH); 3.26 (m, 2H, $NHCH_2$); 3.83 (q, 12H, $SiOCH_2$); 6.03 (s, 2H, CONHNH); 6.53 (s, 2H, $CONHCH_2$); 7.52 ppm (s, 2H, CH_2NH). Elemental Anal. Calc. for $C_{21}H_{48}N_6O_8SSi_2$: C, 41.98; H, 8.05; N, 13.99. Found: C, 41.91; H, 8.26; N, 13.88%.

2.2.3. Synthesis of the molecular hybrid materials containing lanthanide ions (TCH–Si–Ln, TCH–Si–Ln–Bipy, TCH–Si–Ln–Phen, Ln = Eu or Tb)

The hybrid materials were prepared by a typical procedure as follows: the precursor TCH–Si and the second ligands (free for TCH–Si–Ln, 2,2′-bipyridyl for TCH–Si–Ln–Bipy and 1,10-phenanthroline for TCH–Si–Ln–Phen) were dissolved in *N*,*N*-dimethyl formamide (DMF) solution, and then an appropriate amount of $Ln(NO_3)\cdot 6H_2O$ was added. The mixture was kept under room temperature for 3 h, and then TEOS and H_2O were added while stirring. The mole ratio of $Ln(NO_3)\cdot 6H_2O$/TCH–Si/Bipy (or Phen)/TEOS/H_2O was 1:3:1:6:24. When the addition of the TEOS and H_2O were complete, one drop of 20% hydrochloric acid was added to promote hydrolysis. After the treatment of hydrolysis for 8 h, an appropriate amount of hexamethylenetetramine was added to adjust the pH value of 6–7. The resulting mixture was agitated magnetically to achieve a single phase, after that, thermal treatment was performed at 343 K in a covered Teflon beaker for about 6 days until the sample solidified. The obtained gels were washed with ethanol and dried at 363 K for another 3 days. The final molecular hybrid materials were collected as monolithic bulks and were ground into powdered materials for the further studies.

2.3. Physical measurements

All measurements were completed under room temperature. ^{1}H NMR spectra were recorded on a Bruker AVANCE-500 spectrometer with tetramethylsilane (TMS) as internal reference. FT-IR spectra were measured within the 4000–400 cm^{-1} region on a Nicolet model 5SXC spectrophotometer with the KBr pellet technique. Scanning electronic microscope (SEM) images were obtained with a Philips XL-30. Elemental analyses were performed on a VarioEL III O-Element Analyzer system. The X-ray diffraction (XRD) measurements were carried out on powdered samples via a BRUKER D8 diffractometer (40 mA/40 kV) using monochromated Cu Kα1 radiation (λ = 1.54 Å) over the 2θ range of 10°–70°. Differential scanning calorimetry (DSC) and thermogravimetric analysis (TGA) were performed on a NETZSCH STA 449C with a heating rate of 10 K/min under a nitrogen atmosphere (flow rate: 40 mL/min). Reflectivity spectra were recorded on a Bws003 spectrometer equipped with a diffuse reflectance accessory. Fluorescence excitation and emission spectra were obtained on a RF-5301 spectrophotometer with 1.5 nm excitation and 3.0 nm emission slits.

3. Results and discussion

3.1. Organic compound TCH and the silylated precursor TCH–Si

^{1}H NMR spectra relative to the organic compound TCH and the silylated precursor TCH–Si are in full agreement with their

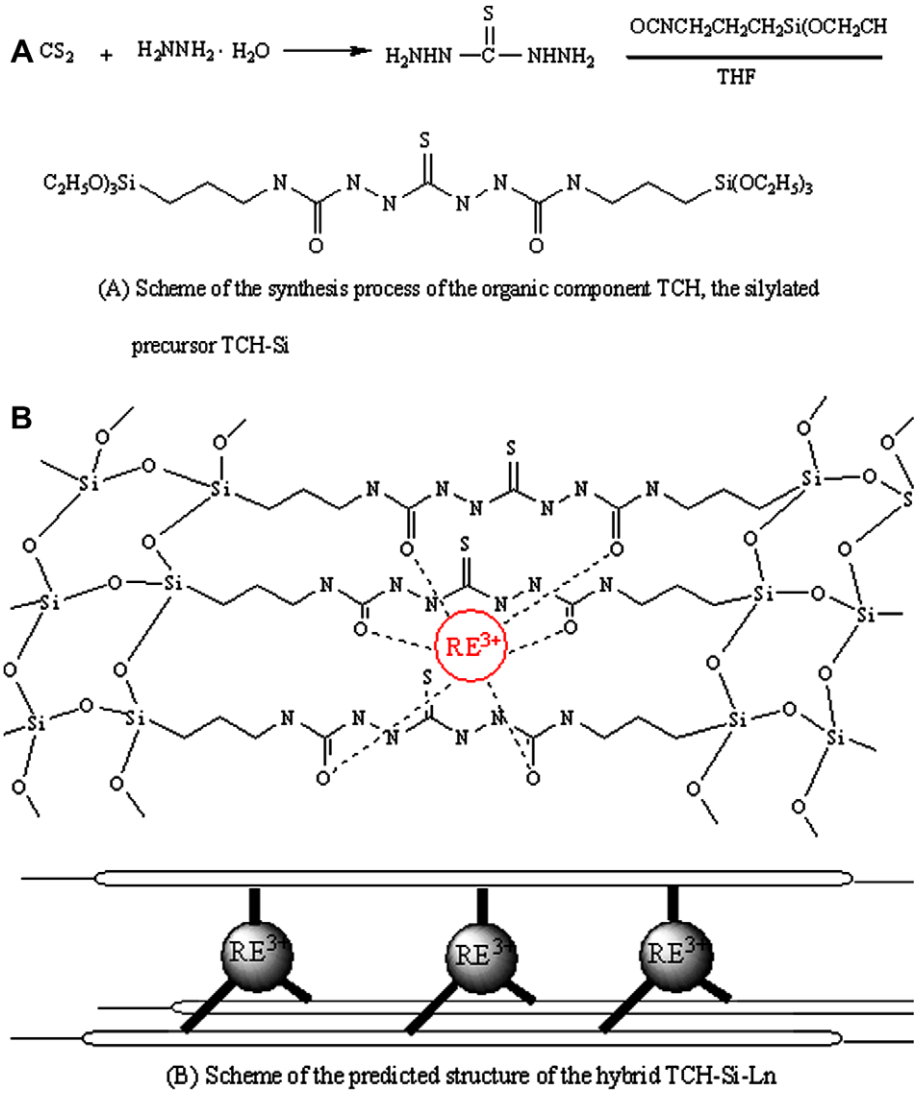

Fig. 1. Scheme of the synthesis process of the organic component TCH, the silylated precursor TCH–Si (A) and the predicted structure of the hybrid TCH–Si–Ln (B).

proposed structures. As detailed in Section 2, ^{1}H NMR chemical shift observed for amino group attributed to –CONH– group, together with the disappearance of the signal of NH_2 group, indicates the accomplishment of the hydrogen-transfer reaction between amino group and the TESPIC. Furthermore, integration of the ^{1}H NMR signal corresponding to ethoxy group shows that no hydrolysis of the precursor occurred during the grafting reaction.

The synthesis of silylated precursor TCH–Si can also be confirmed by the FT-IR. The assignments of the main infrared absorption bands of TCH and TCH–Si are shown in Table 1. The grafting reaction of TCH with TESPIS can be proved by the presence of a series of strong bands at 2975, 2928, 2886 cm^{-1}, which are originating from the vibrations of methylene –$(CH_2)_3$– group. Moreover, the disappearance of the stretch vibration of the absorption peaks located at 2250–2275 cm^{-1} for N=C=O of TESPIC indicate that TESPIC has been completely take part in the grafting reaction with the organic compound TCH. Besides, the stretching vibration of Si–C located at about 1108 cm^{-1}, and the stretching

Table 1
Assignments of the main infrared absorption bands for TCH, TCH–Si and the corresponding hybrids TCH–Si–Eu, TCH–Si–Tb, TCH–Si–Eu–Bipy, TCH–Si–Tb–Bipy, TCH–Si–Eu–Phen, TCH–Si–Tb–Phen.

Compounds	ν(OH) (cm^{-1})	ν(NH_2) (cm^{-1})	ν(CH_2) (cm^{-1})	ν(C=O) (cm^{-1})	ν(Si–C) (cm^{-1})	ν δ(Si–O) (cm^{-1})
TCH		3271 3202				
TCH–Si			2975, 2928, 2886	1678	1198	1108, 1072, 459
TCH–Si–Eu	3427		2966, 2932, 2883	1658	1195	1107, 1079, 462
TCH–Si–Tb	3425		2968, 2930, 2887	1660	1196	1109, 1072, 463
TCH–Si–Eu–Bipy	3422		2971, 2928, 2885	1657	1198	1108, 1075, 465
TCH–Si–Tb–Bipy	3428		2965, 2926, 2886	1653	1200	1106, 1071, 462
TCH–Si–Eu–Phen	3421		2963, 2930, 2884	1656	1194	1109, 1075, 468
TCH–Si–Tb–Phen	3432		2970, 2937, 2885	1652	1198	1110, 1073, 466

vibration of Si–O at 1108 and 1072 cm^{-1}, together with the bending vibration at about 460 cm^{-1} indicate the absorption of the siloxane bonds.

3.2. Hybrid materials (TCH–Si–Ln, TCH–Si–Ln–Phen, TCH–Si–Ln–Bipy, Ln = Eu or Tb)

All of the obtained hybrid materials were also characterized by infrared spectroscopy. The IR spectra of TCH–Si–Eu (A), TCH–Si–Tb (B), TCH–Si–Eu–Phen (C), TCH–Si–Tb–Phen (D), TCH–Si–Eu–Bipy (E) and TCH–Si–Tb–Bipy (F) and the assignments of main infrared absorption bands are shown in Fig. 2 and Table 1, respectively. The presence of the ν(Si–C) absorption, which are located in 1200–1192 cm^{-1} wavelength range, is consistent with the fact that no (Si–C) bond cleavage occurs [8]. While the absorption of ν(Si–O–Si) located in 1109–1060 cm^{-1} wavelength range indicates the formation of siloxane bonds during the hydrolysis/condensation reactions, which is an initial indication for the formation of the true covalent-bonded molecular hybrid materials. However, in the spectra, the ν(O–H) vibration at around 3420 cm^{-1} can also be observed, which means the existence of residual silanol groups and the presence of H_2O molecule. And the ν(Si–OH) stretching vibration at 956 cm^{-1} is a further evidence of the incompleteness of condensation reactions.

Furthermore, the complexation of Ln^{3+} with the organic compound in all of the hybrids can be clearly shown by infrared spectroscopy. Compared with the silylated precursor TCH–Si, the ν(C=O) vibrations of the –CONH– groups are shifted to lower frequency (from 1678 cm^{-1} in TCH–Si to 1652–1660 cm^{-1} in hybrids, $\Delta\nu$ = 18-26 cm^{-1}). This is ascribe to the complexation of the Ln^{3+} ion with the oxygen atom of the C=O group in hybrids [8].

In most case, surface morphology of materials is of great importance for many technical applications requiring well-defined surface or interfaces. From Fig. 3, the scanning electron micrographs for the hybrid materials demonstrate that a homogeneous system was obtained and no phase separation could be observed. That is, covalent-bonding (Si–O–Si) enhanced the miscibility of the organic compounds and the silica matrixes. They were homogeneously and uniformly dispersed at a molecular level via a self-assemble process during the hydrolysis/polycondensation process so that the inorganic and the organic phases can exhibit their distinct properties together. Fig. 3 shows the selected micrographs for (A) TCH–Si–Eu, (B) TCH–Si–Tb, (C) TCH–Si–Eu–Phen, (D) TCH–Si–Tb–Bipy. From the figure we can see that all the samples show the similar

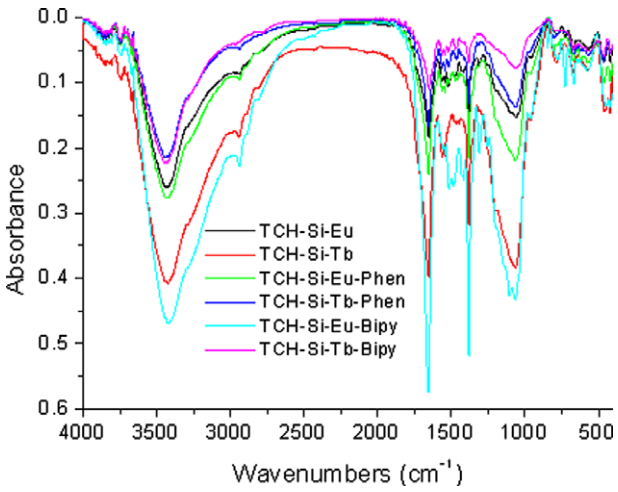

Fig. 2. Infrared spectra of TCH–Si–Eu, TCH–Si–Tb, TCH–Si–Eu–Phen, TCH–Si–Tb–Phen, TCH–Si–Eu–Bipy and TCH–Si–Tb–Bipy in the 4000–400 cm^{-1} range.

microstructures with some chainlike structures which appear like the trunk of pine trees arranged quite regularly on the slippery and clean surfaces of the hybrid materials.

Basically, the sol–gel synthesis of organic–silica hybrid materials mainly involves three steps, that is, hydrolysis, condensation and polycondensation [34]. As far as this three-step process is concerned, the silylated precursor TCH–Si and TEOS are firstly hydrolysed to yield reactive silanol groups. After the initial hydrolysis step, condensation reaction possibly takes place between ethoxy–ethoxy, silanol–silanol and ethoxy–silanol groups, leading to the formation of siloxane chains. The further hydrolysis of the remaining alkoxy groups and polycondensation (or gelation) between chains gives rise to a three-dimensional, crosslinked solid network of siloxane (Si–O–Si). In fact, these three steps cannot be totally isolated, they proceed in parallel rather than in sequence. Their relative rates determine the final structure of the wet silica gel [35]. During the sol–gel process, the type of solvent, pH value, reactant ratios, temperature and the type of catalyst are major factors affecting the relative rates of hydrolysis and condensation reactions, and thus determine the ultimate morphology of the formed materials. In this paper, we select the similar synthesis conditions of the sol–gel technology, such as the reaction temperature, type of solvent, catalyst, and so on. We obtained the similar microstructures for all the hybrid materials. Regarding that the TCH–Si complex has many NH groups, the structure is probably to form a colloidal particles chain, which can compete with the construction of a network structure of Si–O–Si for the hydrolysis and polycondensation process of silica. In terms of the different steric effects and the relative rates, the trunk structure was achieved for the dominant growth along the TCH–Si colloidal particles chain. In consideration of the discussion mentioned above, together with the infrared spectroscopy and other references previously reported [8,36], the resulting predicted structure of the hybrid TCH–Si–Ln is shown in Fig. 1B as an example. However, the structure analysis is one of the most difficult problems in studying the organic–silica hybrid molecular materials. There is but scarce information available about their structure and about the processes that occur during their formation, which could be of great importance for further investigations.

An attempt for homogeneity was made to estimate the crystallinity of hybrids by the powder XRD measurement. The X-ray diffraction patterns of the hybrid materials TCH–Si–Eu, TCH–Si–Tb, TCH–Si–Eu–Phen, TCH–Si–Tb–Phen, TCH–Si–Eu–Bipy and TCH–Si–Tb–Bipy reproduced in Fig. 4 reveal that all the materials are totally amorphous. The absence of any crystalline regions in these samples is due to the presence of organic chains in the host inorganic framework [37]. All the diffraction curves show similar broad amorphous halos, with angel 2θ centered around 22.6°, which is deriving from homogeneously silica matrix [38]. The structural unit distance, calculated using the Bragg law, is approximately 3.91 Å. This may be ascribed to the coherent diffraction of the siliceous backbone of the hybrids. By comparison with all patterns, it seems that the introducing of the second ligands (Bipy or Phen) has no influence on the disorder structure of the siliceous skeleton. In addition, none of the hybrid materials contains measurable amounts of phases corresponding to the pure organic compound or free RE nitrate, which is a further indication for the formation of the true covalent-bonded molecular hybrid materials.

To examine the thermal properties of the hybrid materials, differential scanning calorimetry (DSC) and thermogravimetric analysis (TGA) were performed on all of the amorphous materials. Fig. 5 shows the DSC and TG curves of the hybrids TCH–Si–Eu as an example. There are two main degradation steps can be obviously observed from the TG and DSC curves. The first step of weight loss (about 17.0%) from 200 to 350 °C was attributed to the decomposition of organic ingredients, involving Si–C, C–C, and C–N bond

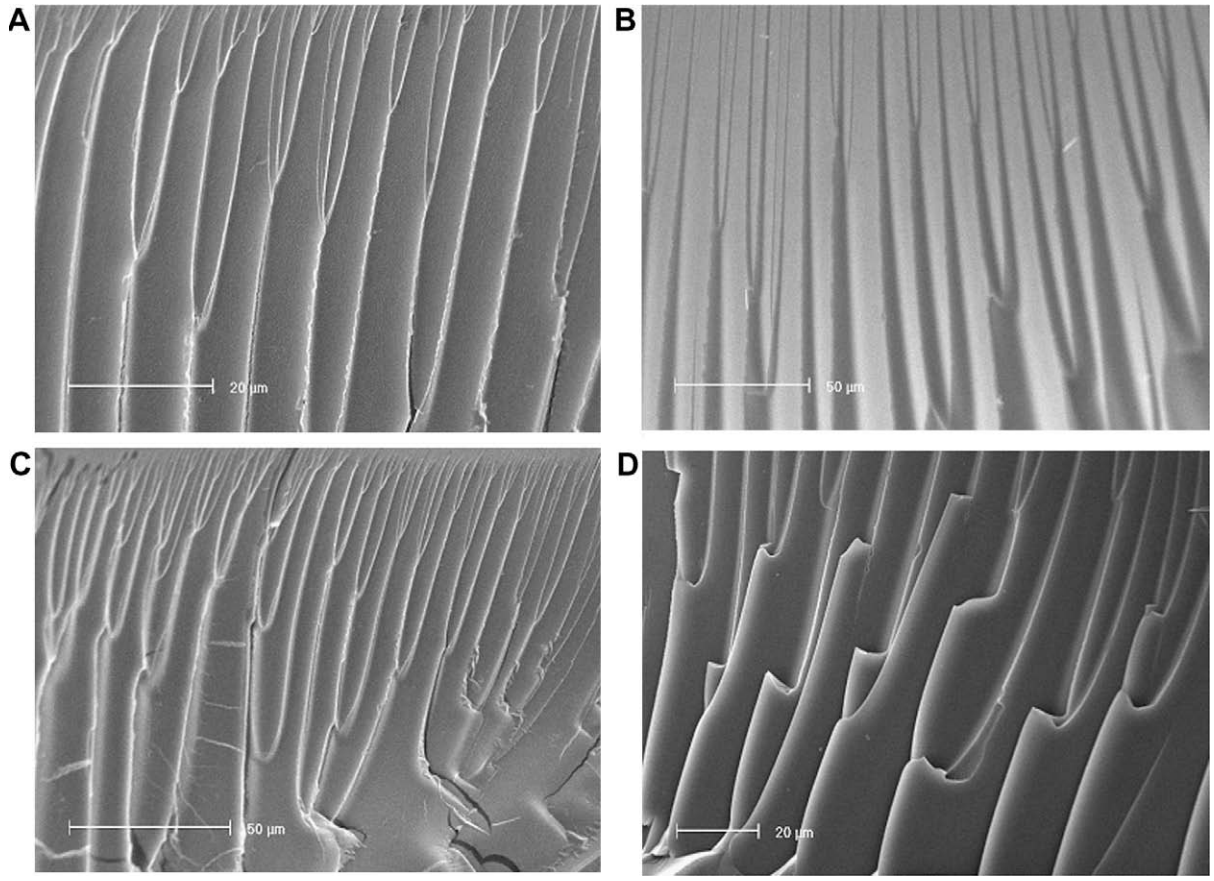

Fig. 3. SEM images for hybrid materials, (A) TCH–Si–Eu, (B) TCH–Si–Tb, (C) TCH–Si–Eu–Phen, (D) TCH–Si–Tb–Bipy.

cleavage [39]. which is an exothermic process observed from the DSC plot. The weight loss beyond 350 °C was ascribed to the releases of water and ethanol formed from the further condensation of silanols in the silica framework. In DSC plot, they express the same thermal change tendency. Because there are even some Si–OH groups on the silica surface and these groups have the ability to undergone condensation to form Si–O–Si networks. The weight loss beyond 450 °C became slightly with the decreasing of the Si–OH groups. The thermal stabilities of this kind of hybrids were largely improved due to the successful incorporation of the silica moiety in the hybrid materials. This improvement of the thermal stability is interpreted by the silica component inducing a protective barrier against thermal degradation for organic species.

Diffuse reflectance experiments were performed on powdered materials for all the materials. Fig. 6 shows the corresponding absorption spectra of (A) TCH–Si–Eu, TCH–Si–Eu–Phen, TCH–Si–Eu–Bipy and (B) TCH–Si–Tb, TCH–Si–Tb–Phen, TCH–Si–Tb–Bipy. All of the spectra exhibit the similar broad absorption bands in

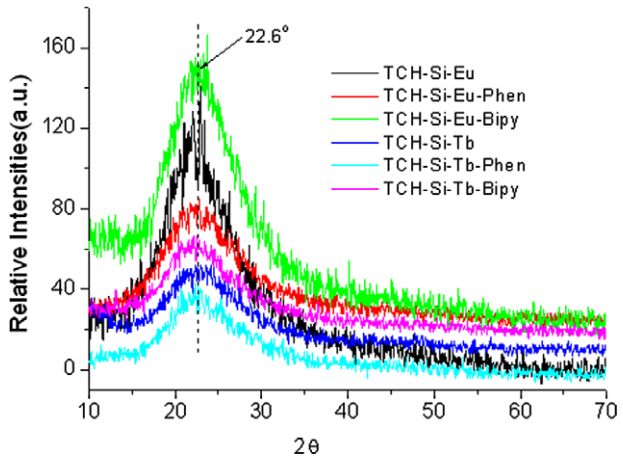

Fig. 4. The X-ray diffraction (XRD) graphs of the hybrids TCH–Si–Eu, TCH–Si–Tb, TCH–Si–Eu–Phen, TCH–Si–Tb–Phen, TCH–Si–Eu–Bipy and TCH–Si–Tb–Bipy.

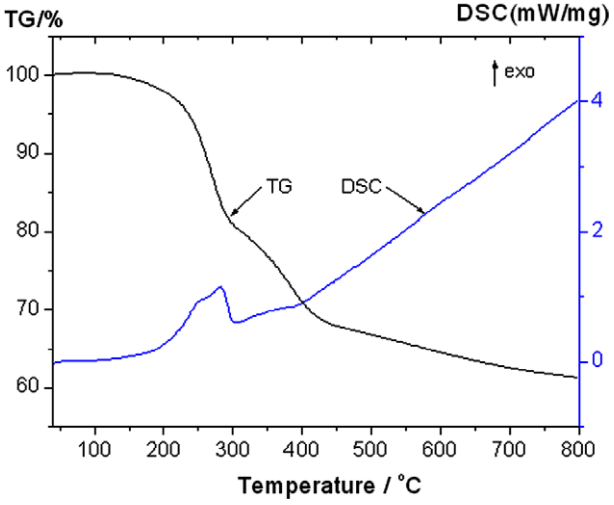

Fig. 5. The selected TG and DSC curves of the hybrids TCH–Si–Eu.

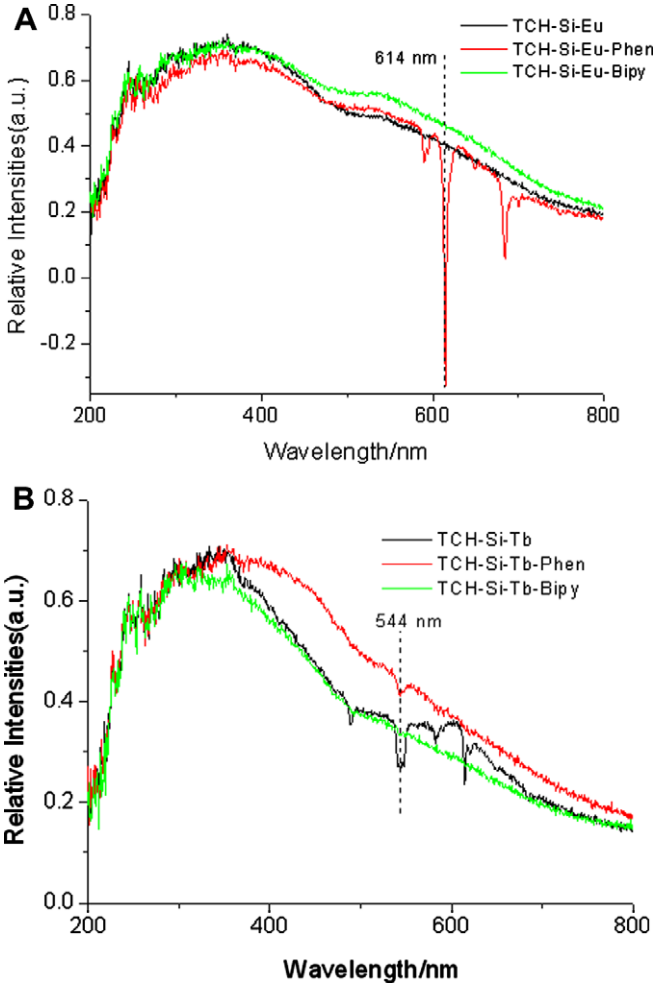

Fig. 6. The ultraviolet–visible diffuse reflection absorption spectra of (A) TCH–Si–Eu, TCH–Si–Eu–Phen, TCH–Si–Eu–Bipy and (B) TCH–Si–Tb, TCH–Si–Tb–Phen, TCH–Si–Tb–Bipy.

the UV–Vis range (200–450 nm), which partially overlap with the fluorescence excitation spectra (wide bands at 280–370 nm in (A) and 250–380 nm in (B)) in Fig. 6. This absorption band may be ascribed to the transition from the ground state of to the first excited state ($S_0 \rightarrow S_1$) of the organic ligand. According to Dexter's exchange energy-transfer theory: the matching degree between the ligand's triplet state energy and lanthanide iron's emission energy can largely influence the luminescence intensity of hybrid material. From the absorption spectra we can primarily predicted that the energy levels matching degree between TCH–Si and RE ions is suited and appropriate so that the organic ligand can absorb abundant energy in ultraviolet–visible extent and to transfer the energy to the corresponding hybrid materials via an intramolecular energy-transfer process. Then the final hybrid materials can be expected to have strong luminescence, which can be proved by the intension of the peaks in 450–700 nm ranges. The signals of 614 nm in Fig. 6A and 545 nm in Fig. 6B were assigned to the transitions from the $^5D_0 \rightarrow {}^7F_2$ transitions for Eu^{3+} ions and the $^5D_4 \rightarrow {}^7F_5$ transitions for Tb^{3+} ions, respectively. For europium hybrid systems, after the addition of the second ligand 1,10-phenanthroline, the fluorescence emission intensity is largely improved, even the transitions from the $^5D_0 \rightarrow {}^7F_1$ transitions at 590 nm can be clearly seen from the spectra. It is indicate that the addition of the second ligand 1,10-phenanthroline can largely sensitize the emission of Eu^{3+} ions. However, for terbium systems, the fluorescence emission intensities of these kinds of materials are determined in the order: TCH–Si–Tb > TCH–Si–Tb–Phen > TCH–Si–Tb–Bipy, the fluorescence emission intensity is not improved after the addition of the second ligands, this can also be proved by the fluorescence spectra in Fig. 7.

Emission of the RE complexes usually results from the so-called "antenna effect", which is defined as a light conversion process via an energy absorption, energy-transfer and energy emission sequence. In such a process, the emission of RE chelates proceeds through the following steps: (a) energy absorption via a ground singlet-excited singlet transition. (b) non-radiative intersystem crossing from the excited singlet to the triplet states. (c) energy-transfer from the ligands to lanthanide ions, and (d) lanthanide ions emission from the excited states. Fig. 7 shows the excitation and emission spectra of the europium hybrid materials (A) TCH–Si–Eu, TCH–Si–Eu–Phen, TCH–Si–Eu–Bipy and the terbium hybrid materials (B) TCH–Si–Tb, TCH–Si–Tb–Phen, TCH–Si–Tb–Bipy. The excitation spectra were obtained by monitoring the emission of Eu^{3+} or Tb^{3+} at 614 or 545 nm. For Eu^{3+} hybrids, all the systems have similar excitation spectra that were dominated by a broad band from 296 to 365 nm with the maximum peak at about 350 nm. As a result, the emission lines of the hybrid materials were assigned to the characteristic $^5D_0 \rightarrow {}^7F_1$ and $^5D_0 \rightarrow {}^7F_2$ transitions at 590 and 614 nm, respectively, while the emission lines of $^5D_0 \rightarrow {}^7F_3$ and $^5D_0 \rightarrow {}^7F_4$ are too weak to be observed. The $^5D_0 \rightarrow {}^7F_2$ emission around 614 nm is the most predominant transition, which agrees with the amorphous characters of the hybrid materials. From the excitation spectra, we can see that the

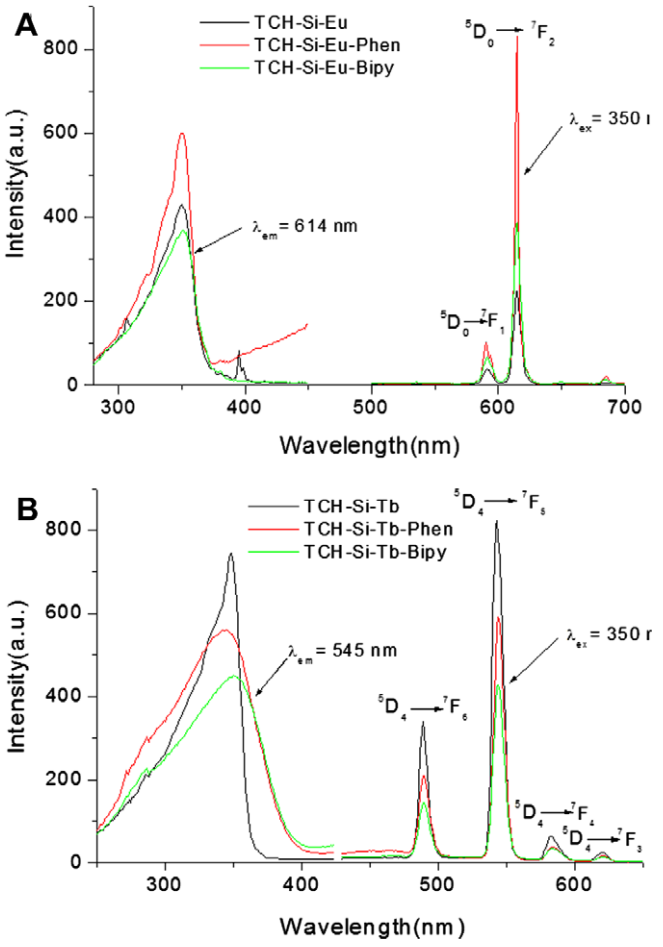

Fig. 7. The excitation and emission spectra of the europium hybrid materials (A) TCH–Si–Eu, TCH–Si–Eu–Phen, TCH–Si–Eu–Bipy and the terbium hybrid materials (B) TCH–Si–Tb, TCH–Si–Tb–Phen, TCH–Si–Tb–Bipy.

Table 2
The luminescence efficiencies and lifetimes for the europium hybrid materials TCH–Si–Eu, TCH–Si–Eu–Bipy and TCH–Si–Eu–Phen.

Hybrids	ν_{01} (cm^{-1})[a]	ν_{02} (cm^{-1})[a]	A_{0J} (s^{-1})	A_{exp} (s^{-1})	A_{rad} (s^{-1})	A_{nrad} (s^{-1})	T (μs)[b]	η (%)
TCH–Si–Eu	16 978	16 313	50 250	2457	300	2157	407	12.2
TCH–Si–Eu–Bipy	16 978	16 313	50 290	1709	340	1369	585	20.0
TCH–Si–Eu–Phen	16 978	16 313	50 421	1340	471	869	746	35.1

[a] The energies of the $5D_0 \rightarrow {}^7F_J$ transitions (ν_{0J}).
[b] For $^5D_0 \rightarrow {}^7F_2$ transition of Eu^{3+}.

fluorescence emission intensities of these kinds of materials are determined in the order: TCH–Si–Eu–Phen > TCH–Si–Eu–Bipy > TCH–Si–Eu, which indicate that the second ligands 1,10-phenanthroline and 2,2′-bipyridyl can efficiently sensitize the luminescence of Eu^{3+} ions. For Tb^{3+} hybrids, a broad band centered at around 347 nm was observed in the excitation spectra and as a result, the emission lines were assigned to the $^5D_4 \rightarrow {}^7F_J$ transitions located at 490, 544, 587 and 622 nm, for J = 6, 5, 4 and 3, respectively. The most striking green fluorescence ($^5D_4 \rightarrow {}^7F_5$) was observed due to the fact that this emission is the most intense one. Corresponding to the emission spectra of Eu^{3+} hybrids, the fluorescent intensities of Tb^{3+} hybrids change with the sequence: TCH–Si–Tb > TCH–Si–Tb–Phen > TCH–Si–Tb–Bipy. The enhancement of the fluorescence intensities after the addition of the second ligands was not observed in the terbium systems. To further investigate the luminescence efficiency of these covalent hybrids, we selectively determined the emission quantum efficiencies of the $^5D_0$ excited state of europium ion for Eu^{3+} hybrids on the basis of the emission spectra and lifetimes of the $^5D_0$ emitting level. The detailed principles and methods were adopted from Refs. [40–48] and the quantum efficiencies of the europium hybrid materials are shown in Table 2, the value η mainly depends on the values of lifetime and the red/orange ratio (I_{02}/I_{01}). The quantum efficiencies of the europium hybrid materials can be determined in the order: TCH–Si–Eu–Phen > TCH–Si–Eu–Bipy > TCH–Si–Eu. So we can see that the second ligand, especially Phen, is the better ligand to sensitize the emission of the Eu^{3+} ions. Furthermore, the quantum efficiencies of TCH–Si–Eu–Phen (35.1%) hybrid systems are much higher than the hybrid materials with functional Calix[4]arene organic ingredients (below 17%) [49], or those with functionalized thiosalicylic acids (below 21%) [30] in our recent work. This may because the higher coordination atoms can be provided by this kind of hybrids after the addition of Phen, and thus the more stable eightfold-coordinated structure with Ln^{3+} ions can effectively reduce of the quenching effect by –OH– group. Meanwhile, the synthesis process can be easily applied to other organic ligands and to different alkoxysilanes, we may expect to obtain stable and efficient hybrid materials in optical or electronic areas for the desired properties can be tailored by an appropriate choice of the precursors and the addition of the second ligands.

4. Conclusions

In summary, compared with the conventional doping systems, we have successfully prepared three types of rare-earth/inorganic/organic covalent-bonded hybrid materials (TCH–Ln, TCH–Si–Ln–Phen and TCH–Si–Ln–Bipy) using TCH–Si compound as a bridge molecule which can both coordinate to rare-earth ions (Eu^{3+} and Tb^{3+}) and form an inorganic Si–O–Si network with tetraethoxysilane (TEOS). By controlling the conditions of the sol–gel technology, we obtained all of these hybrid materials with homogeneous chain microstructure, suggesting the occurrence of self-assembly of the inorganic network and organic chain. Measurements of the photoluminescent properties show that the ternary europium hybrids present stronger luminescent intensities than the binary hybrids, indicating that the introduction of the second ligands can sensitize the luminescence emissions of the europium hybrid systems. However, this sensitization effect was not observed in the terbium hybrid systems. This may be ascribe to the energy match between the ligands triplet state and the resonant emissive energy level of the central Eu^{3+} ions not as proper as for Tb^{3+} ions. As the synthesis process can be easily applied to other organic ligands and to different alkoxysilanes, we may expect to obtain stable and efficient hybrid materials in optical or electronic areas because the desired properties can be tailored by an appropriate choice of the precursors. However, the structure of the hybrid materials and the processes that occur during the sol–gel technology need further fundamental investigations.

Acknowledgements

This work was supported by the National Natural Science Foundation of China (20971100) and Program for New Century Excellent Talents in University (NCET-08-0398).

References

[1] K. Kuriki, Y. Koike, Y. Okamoto, Chem. Rev. 102 (2002) 2347–2356.
[2] L.H. Sloff, A. van Blaaderen, A. Polman, G.A. Hebbink, S.I. Klink, F.C.J.M. van Veggel, D.N. Reinhoudt, J.W. Hofstraat, J. Appl. Phys. 91 (2002) 3955–3980.
[3] T. Oyamada, Y. Kawamura, T. Koyama, H. Sasabe, C. Adachi, Adv. Mater. 16 (2004) 1082–1086.
[4] G.F. DeSá, O.L. Malta, C. De Mello Donegá, A.M. Simas, R.L. Longo, P.A. Santa-Cruz, E.F. da Silva Jr., Coord. Chem. Rev. 196 (2000) 165–195.
[5] N. Sabbatini, M. Guardingli, J.M. Lehn, Coord. Chem. Rev. 123 (1993) 201–228.
[6] S.I. Klink, L. Grave, D.N. Reinhoudt, F.C.J.M. van Veggel, M.H.F. Werts, F.A.J. Geurts, J.W. Hofstraat, J. Phys. Chem. A 104 (2000) 5457–5468.
[7] N.S. Baek, Y.H. Kim, S.G. Roh, B.K. Kwak, H.K. Kim, Adv. Funct. Mater. 16 (2006) 1873–1882.
[8] A.C. Franville, D. Zambon, R. Mahiou, Chem. Mater. 12 (2000) 428–435.
[9] F.Y. Liu, L.S. Fu, H.J. Zhang, New J. Chem. 27 (2003) 233–235.
[10] M. Schneider, K. Müllen, Chem. Mater. 12 (2000) 352–362.
[11] C. Sanchez, F. Ribot, New J. Chem. 18 (1994) 1007–1047.
[12] J. Wen, G.L. Wilkes, Chem. Mater. 8 (1996) 1667–1681.
[13] P.G. Romero, Adv. Mater. 13 (2001) 163–174.
[14] C. Guizard, P. Lacan, New J. Chem. 18 (1994) 1097–1107.
[15] K.J. Shea, D.A. Loy, Chem. Mater. 13 (2001) 3306–3319.
[16] R.J.P. Corriu, D. Leclercq, Angew. Chem., Int. Ed. Engl. 35 (1996) 1420–1436.
[17] R.J.P. Corriu, Angew. Chem., Int. Ed. 39 (2000) 1376–1398.
[18] H.R. Li, J. Lin, H.J. Zhang, L.S. Fu, Chem. Mater. 14 (2002) 3651–3655.
[19] K. Binnemans, Chem. Rev. 109 (2009) 4283–4374.
[20] L.D. Carlos, R.A. Sá Ferreira, R.N. Pereira, M. Assuncao, V.D. Bermudez, J. Phys. Chem. B 108 (2004) 14924–14932.
[21] L.H. Wang, W. Wang, W.G. Zhang, E.T. Kang, W. Huang, Chem. Mater. 12 (2002) 2212–2219.
[22] L.D. Carlos, R.A. Sá Ferreira, V. de Zea Bermudez, S.J.L. Ribeiro, Adv. Mater. 21 (2009) 509–534.
[23] D.W. Dong, S.C. Jiang, Y.F. Men, X.L. Ji, B.Z. Jiang, Adv. Mater. 12 (2000) 646–649.
[24] Q.M. Wang, B. Yan, J. Mater. Chem. 14 (2004) 2450–2454.
[25] Q.M. Wang, B. Yan, Cryst. Growth Des. 5 (2005) 497–503.
[26] Q.M. Wang, B. Yan, J. Organomet. Chem. 691 (2006) 545–550.
[27] Q.M. Wang, B. Yan, J. Organomet. Chem. 691 (2006) 3567–3573.
[28] J.L. Liu, B. Yan, J. Phys. Chem. B 112 (2008) 10898–10907.
[29] H.F. Lu, B. Yan, J. Non-Cryst. Solids 352 (2006) 5331–5336.
[30] B. Yan, H.F. Lu, Inorg. Chem. 47 (2008) 5601–5611.
[31] J.L. Liu, B. Yan, J. Phys. Chem. C 112 (2008) 14168–14178.
[32] Q.M. Wang, B. Yan, Cryst. Growth Des. 8 (2008) 1484–1489.
[33] D.D. Perrin, W.L.F. Armarego, D.R. Perrin, Purification of Laboratory Chemicals, Pergamon Press, Oxford, 1980.

[34] A. Malik, Electrophoresis 23 (2002) 3973–3992.
[35] A.M. Siouffi, J. Chromatogr., Sect. A 1000 (2003) 801–818.
[36] A.C. Franville, D. Zambon, R. Mahiou, S. Chou, Y. Troin, J.C. Cousseins, J. Alloys Compd. 275–277 (1998) 831–834.
[37] B. Yan, X.F. Qiao, J. Phys. Chem. B 111 (2007) 12362–12374.
[38] F.X. Qiu, Z.L. Da, D.Y. Yang, G.R. Cao, P.P. Li, Dyes Pigm. 77 (2008) 564–569.
[39] P. Tien, L.K. Chau, Chem. Mater. 11 (1999) 2141–2147.
[40] O.L. Malta, M.A. Couto dos Santos, L.C. Thompson, N.K. Ito, J. Lumin. 69 (1996) 77–84.
[41] O.L. Malta, H.F. Brito, J.F.S. Menezes, F.R. Goncaülves e Silva, S. Alves Jr., F.S. Farias Jr., A.V.M. de Andrade, J. Lumin. 75 (1997) 255–268.
[42] L.D. Carlos, Y. Messaddeq, H.F. Brito, R.A. Sá Ferreira, V. de Zea Bermudez, S.J.L. Ribeiro, Adv. Mater. 12 (2000) 594–598.
[43] R.A. Sá Ferreira, L.D. Carlos, R.R. Goncaülves, S.J.L. Ribeiro, V. de Zea Bermudez, Chem. Mater. 13 (2001) 2991–2998.
[44] P.C.R. Soares-Santos, H.I.S. Nogueira, V. Felix, M.G.B. Drew, R.A. Sá Ferreira, L.D. Carlos, T. Trindade, Chem. Mater. 15 (2003) 100–108.
[45] E.E.S. Teotonio, J.G.P. Espinola, H.F. Brito, O.L. Malta, S.F. Oliveria, D.L.A. de Foria, C.M.S. Izumi, Polyhedron 21 (2002) 1837–1844.
[46] S.J.L. Ribeiro, K. Dahmouche, C.A. Ribeiro, C.V. Santilli, S.H.J. Pulcinelli, J. Sol–Gel Sci. Technol. 13 (1998) 427–432.
[47] M.H.V. Werts, R.T.F. Jukes, J.W. Verhoeven, Phys. Chem. Chem. Phys. 4 (2002) 1542–1548.
[48] C.Y. Peng, H.J. Zhang, J.B. Yu, Q.G. Meng, L.S. Fu, H.R. Li, L.N. Sun, X.M. Guo, J. Phys. Chem. B 109 (2005) 15278–15287.
[49] H.F. Lu, B. Yan, J.L. Liu, Inorg. Chem. 48 (2009) 3966–3975.